Analysis of a Longitudinal Gyroelectric Discontinuity Inside a Fiber Waveguide

P. G. COTTIS AND NIKOLAOS K. UZUNOGLU, MEMBER, IEEE

Abstract—**The scattering of guided electromagnetic waves from a finite-length longitudinal gyroelectric discontinuity inside a fiber waveguide is treated analytically. An integral equation approach is employed to formulate the corresponding boundary-value problem. The induced field inside the gyroelectric discontinuity region is expanded into a Fourier-type series in terms of the well-known cylindrical waves *M* and *N* plus a purely longitudinal wave *Q*. Then the method of moments is applied to decouple the basic integral equation. The resulting infinite coupled system of equations is truncated and solved numerically. After determining the field inside the discontinuity, the scattered far field inside the dielectric-rod waveguide is computed by employing a steepest descent integration technique. Numerical results for the scattering coefficients of an incident HE_{11} dominant mode are obtained. Finally, design principles are discussed for practical components based on the treated longitudinal gyroelectric discontinuity.**

I. INTRODUCTION

THE DEVELOPMENT OF low-loss optical fiber waveguides and the increasing use of dielectric waveguides in millimetric wavelengths has created the necessity for developing new circuit components associated with these new transmission lines. In the development of active or nonreciprocal components such as modulators, switches, isolators, etc., several physical phenomena are exploited. One of these phenomena is the magnetooptic effect (in particular, the Faraday rotation of the polarization plane). In recent years, there have been several analytical treatments for the use of anisotropies in integrated optics thin-film waveguides [1]–[3]. A bulk-type optical isolator using the Faraday rotation has been reported [4] for the $\lambda = 1.15$-μm radiation wavelength. Considering the cylindrical dielectric-rod waveguide geometry, it seems that a natural way to pass the guided wave through a Faraday rotation medium is to introduce a finite-length longitudinal gyrotropy along the waveguide axis. If such a nonreciprocal circuit element could be realized, then all the benefits [2] of the waveguide-type modulators could be exploited to design active optical devices. The geometry of the longitudinal gyroelectric discontinuity is shown in Fig. 1, where the fiber waveguide radius and dielectric permittivity are shown by b and $\epsilon_r\epsilon_0$, respectively. The gyroelectric discontinuity, occupying the region $-\alpha < z < \alpha$ of the infinite cylinder, is characterized by a tensor dielectric permittivity

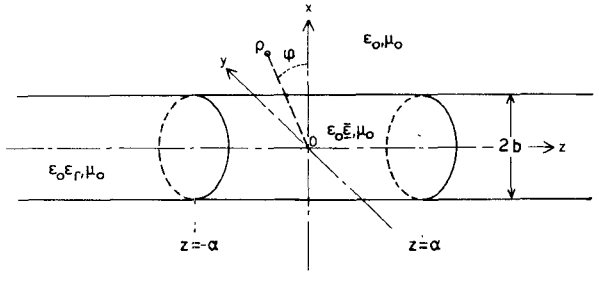

Fig. 1. Gyroelectric discontinuity in a dielectric waveguide.

$$\bar{\epsilon} = \epsilon_0 \begin{bmatrix} \epsilon_1 & -i\epsilon_2 & 0 \\ i\epsilon_2 & \epsilon_1 & 0 \\ 0 & 0 & \epsilon_3 \end{bmatrix} \tag{1}$$

and the whole space is assumed to be magnetically homogeneous, i.e., $\mu = \mu_0$, where ϵ_0 and μ_0 are the free-space permittivity and permeability constants, respectively. The free-space wavenumber for the $\rho > b$ (see Fig. 1) outer region is shown by $k_0 = \omega\sqrt{\epsilon_0\mu_0}$, where ω is the angular frequency of the electromagnetic field. According to (1), the anisotropy axis is assumed to be along the z-axis. This occurs when the externally applied static field, biasing the gyroelectric medium, is parallel to the waveguide axis.

Assume an incident guided wave $\boldsymbol{E}_0(r)$ either from the left or the right (Fig. 1) to the gyroelectric discontinuity region. Then the scattering will take place at the discontinuity region creating forward and backward guided waves and partial radiation of the incident energy. In order to describe this process, an integral equation approach in conjunction with the Green's function method is employed in this paper. The dyadic Green's theorem, when applied to formulate the corresponding boundary-value problem, results in a volume integral equation for the unknown electric field inside the gyroelectric discontinuity. The kernel of this integral equation is the Green's dyadic for a dielectric rod expressed in terms of cylindrical vector wave functions. The unknown interior field for the gyroelectric medium is expressed as a superposition of the cylindrical waves *M* and *N* and a longitudinal wave *Q*. This expansion satisfies the Maxwell equations for the gyroelectric medium. Sub-

Manuscript received June 10, 1985; revised November 14, 1985.
The authors are with the Department of Electrical Engineering, National Technical University of Athens, Athens 10682, Greece.
IEEE Log Number 8407178.

stituting this expansion into the basic integral equation, with

$$C_m^{(j)}(x) = \begin{cases} J_m(x) & (j=1, \text{Bessel function}) \\ Y_m(x) & (j=2, \text{Neumann function}) \\ J_m(x) + iY_m(x) = H_m(x) & (j=3, \text{Hankel function}) \end{cases}$$

performing the necessary integrations and applying a method of moments procedure, an infinite set of equations is obtained for the unknown expansion coefficients of the interior field. Truncation and the numerical solution of this set of equations determines approximately the field induced inside the gyroelectric region. Application of the steepest descent integration technique for $z \to \pm\infty$ along the fiber axis yields asymptotic expressions for the scattering coefficients.

It should be noted that the solution developed in this paper is directly applicable to isotropic longitudinal discontinuities by assuming in (1) $\epsilon_1 \to \epsilon_3$ and $\epsilon_2 \to 0$. This is a commonly encountered problem in many practical fiber guide junction or splicing points.

In the following, a harmonic $\exp(-i\omega t)$ time dependence is assumed for the electromagnetic field quantities and is suppressed throughout the analysis.

II. Mathematical Formulation of the Problem

In this paper, a Green's function formulation is used as in [5], where the scattering from a spherical inhomogeneity inside a dielectric waveguide is treated analytically. In the following analysis, the dielectric waveguide is assumed to be a single mode carrying only the $HE_{\pm 11}$ dominant mode. Then the guided incident wave $\boldsymbol{E}_0^m(\boldsymbol{r})$ inside the guide could be written as a linear combination of transverse electric (TE) $\boldsymbol{M}$ and magnetic (TM) $\boldsymbol{N}$ waves in the form [5]

$$\boldsymbol{E}_0^m(\boldsymbol{r}) = \boldsymbol{M}_{m,v}^{(1)}(\boldsymbol{r}, k_1) + m\delta_1(v)\boldsymbol{N}_{m,v}^{(1)}(\boldsymbol{r}, k_1) \tag{2}$$

with $m = +1$ or -1, $\rho < b$ (see Fig. 1), v is the propagation constant of the HE_{11} mode, and $\delta_1(v)$ is a known factor as defined below. The conventional cylindrical wave functions appearing in (2) are defined as

$$\boldsymbol{M}_{m,k}^{(j)}(\boldsymbol{r}, k_1) = \left(\frac{im}{\rho} C_m^{(j)}(\alpha_1\rho)\hat{\rho} - \frac{\partial C_m^{(j)}(\alpha_1\rho)}{\partial\rho}\hat{\varphi} \right) e^{im\varphi} e^{ikz} \tag{3}$$

$$\boldsymbol{N}_{m,k}^{(j)}(\boldsymbol{r}, k_1) = \frac{1}{k_1}\left(ik\frac{\partial C_m^{(j)}(\alpha_1\rho)}{\partial\rho}\hat{\rho} - \frac{mk}{\rho} C_m^{(j)}(\alpha_1\rho)\hat{\varphi} + \alpha_1^2 C_m^{(j)}(\alpha_1\rho)\hat{z} \right) e^{im\varphi} e^{ikz} \tag{4}$$

$\alpha_1 = (k_1^2 - k^2)^{1/2}$, $k_1 = k_0\sqrt{\epsilon_r}$, $\boldsymbol{r} = \rho\hat{\rho} + z\hat{z}$, (ρ, φ, z) being the cylindrical coordinates and $m = 0, \pm 1, \pm 2, \pm 3, \ldots$. In the following analysis, the $\boldsymbol{M}$ and $\boldsymbol{N}$ vector wave functions are employed extensively to express electromagnetic fields. The weighting factor in front of the $\boldsymbol{N}_{m,v}$ wave in (2), as given in [5], is written as

$$\delta_1(v) = \frac{k_1 b}{v} \frac{\alpha_0 J_1'(\alpha_1 b) H_1(\alpha_0 b) - \alpha_1 J_1(\alpha_1 b) H_1'(\alpha_0 b)}{k_0^2(\epsilon_r - 1) J_1(\alpha_1 b) H_1(\alpha_0 b)} \tag{5}$$

with $\alpha_0 = (k_0^2 - k^2)^{1/2}$.

As the incident wave $\boldsymbol{E}_0^m(\boldsymbol{r})$ impinges on the gyroelectric discontinuity of Fig. 1, secondary fields are induced inside and outside the gyroelectric medium. The superposition of the incident and the secondary electric fields gives the total field $\boldsymbol{E}(\boldsymbol{r})$. Applying the dyadic Green's theorem in a similar manner as in [5, sec. II], an integral expression is obtained for the unknown electric field $\boldsymbol{E}(\boldsymbol{r})$ as

$$\boldsymbol{E}(\boldsymbol{r}) = \boldsymbol{E}_0(\boldsymbol{r}) + k_0^2 \int\int\int_{V_0} \bar{\boldsymbol{G}}(\boldsymbol{r}, \boldsymbol{r}') \cdot \left[(\bar{\epsilon} - \epsilon_r \bar{1}) \cdot \boldsymbol{E}(\boldsymbol{r}') \right] d\boldsymbol{r}' \tag{6}$$

where $\bar{\boldsymbol{G}}(\boldsymbol{r}, \boldsymbol{r}')$ is the dyadic Green's function for the infinite dielectric waveguide in the absence of the gyroelectric discontinuity and $\bar{1}$ is the unit dyadic. The integration is carried out over the gyroelectric region V_0 (Fig. 1). If the observation point $\boldsymbol{r}$ in (6) is restricted inside the volume V_0, then an integral equation is obtained for the unknown electric field $\boldsymbol{E}(\boldsymbol{r})$.

The dyadic Green's function $\bar{\boldsymbol{G}}(\boldsymbol{r}, \boldsymbol{r}')$ is determined by solving the boundary-value problem for the excitation of the dielectric waveguide by an elementary excitation current $\bar{1}\delta(\boldsymbol{r} - \boldsymbol{r}')$, as explained in detail in [5]. The expression given here for the dyadic $\bar{\boldsymbol{G}}(\boldsymbol{r}, \boldsymbol{r}')$ is in a format suitable for the presently treated cylindrical discontinuity geometry. The dyadic Green's function $\bar{\boldsymbol{G}}(\boldsymbol{r}, \boldsymbol{r}')$ is decomposed into two terms as

$$\bar{\boldsymbol{G}}(\boldsymbol{r}, \boldsymbol{r}') = \bar{\boldsymbol{G}}_0(\boldsymbol{r}, \boldsymbol{r}') + \bar{\boldsymbol{G}}_1(\boldsymbol{r}, \boldsymbol{r}') \tag{7}$$

where $\bar{\boldsymbol{G}}_0(\boldsymbol{r}, \boldsymbol{r}')$ corresponds to the free-space Green's dyadic (for an infinite medium with a dielectric permittivity $\epsilon = \epsilon_0\epsilon_r$ and magnetic permeability $\mu = \mu_0$) and $\bar{\boldsymbol{G}}_1(\boldsymbol{r}, \boldsymbol{r}')$ is to take into account the reaction of the dielectric waveguide. The free-space Green's dyadic including the singu-

larity term at $\rho = \rho'$ is written as [6]

$$\bar{G}_0(\boldsymbol{r},\boldsymbol{r}') = \frac{i}{8\pi}\int_{-\infty}^{+\infty} dk \sum_{m=-\infty}^{+\infty} \frac{(-1)^m}{\alpha_1^2} \cdot \begin{cases} \boldsymbol{M}^{(3)}_{m,k}(\boldsymbol{r},k_1)\boldsymbol{M}^{(1)}_{-m,-k}(\boldsymbol{r}',k_1) \\ \quad + \boldsymbol{N}^{(3)}_{m,k}(\boldsymbol{r},k_1)\boldsymbol{N}^{(1)}_{-m,-k}(\boldsymbol{r}',k_1) & (\rho > \rho') \\ \boldsymbol{M}^{(1)}_{m,k}(\boldsymbol{r},k_1)\boldsymbol{M}^{(3)}_{-m,-k}(\boldsymbol{r}',k_1) \\ \quad + \boldsymbol{N}^{(1)}_{m,k}(\boldsymbol{r},k_1)\boldsymbol{N}^{(3)}_{-m,-k}(\boldsymbol{r}',k_1) & (\rho < \rho') \end{cases} - k_1^{-2}\hat{\rho}\hat{\rho}\delta(\boldsymbol{r}-\boldsymbol{r}'). \tag{8}$$

The dyadic $\bar{G}_1(\boldsymbol{r},\boldsymbol{r}')$ term can be written as

$$\begin{aligned}\bar{G}_1(\boldsymbol{r},\boldsymbol{r}') = \frac{i}{8\pi}\int_{-\infty}^{+\infty} dk \sum_{m=-\infty}^{+\infty} \frac{(-1)^m}{\alpha_1^2} \cdot \big[& \alpha(m,k)\boldsymbol{M}^{(1)}_{m,k}(\boldsymbol{r},k_1)\boldsymbol{M}^{(1)}_{-m,-k}(\boldsymbol{r}',k_1) \\ & + b(m,k)\boldsymbol{M}^{(1)}_{m,k}(\boldsymbol{r},k_1)\boldsymbol{N}^{(1)}_{-m,-k}(\boldsymbol{r}',k_1) \\ & + b(m,k)\boldsymbol{N}^{(1)}_{m,k}(\boldsymbol{r},k_1)\boldsymbol{M}^{(1)}_{-m,-k}(\boldsymbol{r}',k_1) \\ & + c(m,k)\boldsymbol{N}^{(1)}_{m,k}(\boldsymbol{r},k_1)\boldsymbol{N}^{(1)}_{-m,-k}(\boldsymbol{r}',k_1)\big] \end{aligned} \tag{9}$$

where the terms $\alpha(m,k)$, $b(m,k)$, and $c(m,k)$ are given in [5, eqs. (19)–(23)].

III. Expansion of the Electric Field Inside the Gyroelectric Medium

In order to solve (6), the unknown electric field ($\boldsymbol{E}(\boldsymbol{r})$) inside the gyroelectric discontinuity should be expanded into a complete set of proper eigenwaves. These eigenwaves are determined by solving the vector wave equation

$$\nabla \times \nabla \times \boldsymbol{E}(\boldsymbol{r}) - k_0^2 \bar{\epsilon}\cdot\boldsymbol{E}(\boldsymbol{r}) = 0 \tag{10}$$

for an infinite medium. Considering the solution of (10) in the Fourier domain, the electric field inside the discontinuity region can be written as

$$\boldsymbol{E}(\boldsymbol{r}) = \int\int_{-\infty}^{+\infty} d\boldsymbol{\xi}_t \sum_{n=-\infty}^{+\infty} \exp(i\boldsymbol{\xi}_n\cdot\boldsymbol{r})\boldsymbol{e}_n(\boldsymbol{\xi}_t) \tag{11}$$

where $\boldsymbol{\xi}_n = \boldsymbol{\xi}_t + \hat{z}k_n$, $k_n = (n\pi/\alpha)$, $\boldsymbol{\xi}_t = \hat{x}\xi_x + \hat{y}\xi_y$ and $\boldsymbol{e}_n(\boldsymbol{\xi}_t)$ is an unknown function to be determined. Substituting (11) into (10), assuming a nontrivial solution for the $\boldsymbol{e}_n(\boldsymbol{\xi}_t)$ vector function and defining $\xi = [\boldsymbol{\xi}_t] = (\xi_x^2 + \xi_y^2)^{1/2}$, a characteristic equation is obtained in the form

$$\epsilon_1\xi^4 + \big(P(\epsilon_1+\epsilon_3) + Q\epsilon_2\big)\xi^2 + \big(P^2 - Q^2\big)\epsilon_3 = 0 \tag{12}$$

where $P = k^2 - k_0^2\epsilon_1$, $Q = k_0^2\epsilon_2$.

The solution of (12) leads to the well-known ordinary and extraordinary waves. The corresponding roots $\xi^2 = \xi_1^2, \xi_2^2$, are the only allowed values for the ξ variable in the expansion (11). Furthermore, (12), being biquadratic in ξ, has symmetric roots shown in the following as $\pm\xi_i$, $i = 1,2$. Notice that these roots are independent of the $\varphi_\xi = \tan^{-1}(\xi_y/\xi_x)$ azimuthal angle. Then the Fourier integral in (11) is rewritten as

$$\boldsymbol{E}(\boldsymbol{r}) = \sum_{i=1}^{2}\int_0^{2\pi} d\varphi_\xi \sum_{n=-\infty}^{+\infty} e^{ik_n z}\cdot e^{i\xi\rho\cos(\varphi-\varphi_\xi)}\xi_i\boldsymbol{e}_{ni}(\varphi_\xi) \tag{13}$$

where $\rho = (x^2+y^2)^{1/2}$, $\varphi = \tan^{-1}(y/x)$ (see Fig. 1) are the polar coordinates. Observe that only the $\xi = \xi_1$ and $\xi = \xi_2$ roots are taken into account, since the symmetric roots are automatically included, when the integration over the φ_ξ variable is performed. If one substitutes (13) into (10), a homogeneous 3×3 linear system of equations is obtained. Then it is possible to express the $e_{xni} = \boldsymbol{e}_{ni}\cdot\hat{x}$ and $e_{yni} = \boldsymbol{e}_{ni}\cdot\hat{y}$ components in terms of the $e_{zni} = \boldsymbol{e}_{ni}\cdot\hat{z}$. Furthermore, expanding the $\exp(i\xi_i\rho\cos(\varphi-\varphi_\xi))$ and $e_{zni}(\varphi_\xi)$ terms in (13) into Fourier series for the φ_ξ variable and properly grouping the terms involved, (13) can be rewritten in terms of the vector eigenwaves as

$$\boldsymbol{E}(\boldsymbol{r}) = \sum_{n=-\infty}^{+\infty}\sum_{i=1}^{2}\sum_{m=-\infty}^{+\infty} c_{m,n,i}\psi_{m,n,i}(\boldsymbol{r}) \tag{14}$$

where

$$\begin{aligned}\psi_{m,n,i}(\boldsymbol{r}) = i^m\big\{ & A_M(n,\xi_i)\boldsymbol{M}^{(1)}_{m,k_n}(\boldsymbol{r},K_i) \\ & + A_N(n,\xi_i)\boldsymbol{N}^{(1)}_{m,k_n}(\boldsymbol{r},K_i) \\ & + A_Q(n,\xi_i)\boldsymbol{Q}^{(1)}_{m,k_n}(\boldsymbol{r},K_i)\big\}\end{aligned} \tag{15}$$

and where $c_{m,n,i}$ are unknown coefficients to be determined and

$$A_M(n,\xi_i) = \frac{k_0^2\epsilon_2 k_n}{D(\xi_i,k_n)} \tag{15b}$$

$$A_N(n,\xi_i) = \frac{\xi_i^2 + k_n^2 - k_0^2\epsilon_1}{D(\xi_i,k_n)} \tag{15c}$$

$$A_Q(n,\xi_i) = \frac{\big(\xi_i^2 + k_n^2 - k_0^2\epsilon_1\big)^2 - k_0^4\epsilon_2^2}{D(\xi_i,k_n)} \tag{15d}$$

$$D(\xi_i,k_n) = \big(k_0^2\epsilon_1 - k_n^2\big)\big(\xi_i^2 + k_n^2 - k_0^2\epsilon_1\big) + k_0^4\epsilon_2^2 \tag{15e}$$

$$K_i = \big(\xi_i^2 + k_n^2\big)^{1/2}.$$

Finally

$$\boldsymbol{Q}^{(1)}_{m,k_n}(\boldsymbol{r},K_i) = \hat{z}J_m(\xi_i\rho)e^{i(m\varphi+k_n z)} \tag{16}$$

is an additional longitudinal wave due to the anisotropy.

IV. Solution of the Integral Equation

In order to determine the electric field inside the gyroelectric discontinuity region, substitute the field representation of (14) into the fundamental integral equation (6). In the first place, it is necessary to compute the $(\bar{\epsilon} - \epsilon_r\bar{1})\cdot\boldsymbol{E}(\boldsymbol{r}')$ term under the integral sign. To do this, (14) is employed for the representation of the electric field. Then the product $(\bar{\epsilon} - \epsilon_r\bar{1})\cdot\psi_{m,n,i}(\boldsymbol{r}')$ is computed. After a series of algebraic manipulations, the $(\bar{\epsilon} - \epsilon_r\bar{1})\cdot\boldsymbol{E}(\boldsymbol{r}')$ term is expressed

as a superposition of the M, N, and Q cylindrical wave functions. This intermediate result has been proved to be critical in the following integral equation solution procedure.

Then the following integrals are encountered for the integration inside the gyroelectric discontinuity volume

$$\begin{matrix} \boldsymbol{I}_{pi}^{(M)}(\boldsymbol{r}) & & \boldsymbol{M}_{m,k_n}^{(1)}(\boldsymbol{r}', K_i) \\ \boldsymbol{I}_{pi}^{(N)}(\boldsymbol{r}) = \iiint_{V_0} d\boldsymbol{r}' \overline{\boldsymbol{G}}_p(\boldsymbol{r}/\boldsymbol{r}') \cdot & & \boldsymbol{N}_{m,k_n}^{(1)}(\boldsymbol{r}', K_i) \\ \boldsymbol{I}_{pi}^{(Q)}(\boldsymbol{r}) & & \boldsymbol{Q}_{m,k_n}^{(1)}(\boldsymbol{r}', K_i) \end{matrix}$$

where $p = 0,1$ and $i = 1,2$. Since $\overline{G}_0$ and $\overline{G}_1$, as given from (8) and (9), respectively, are expressed in terms of the cylindrical wave functions, the orthogonality relations between the M, N, and Q functions are employed when computing the integrals I_{pi}. Furthermore, multiply both sides of the integral (6) with the vector wave function $\psi_{-m',-n',j}(\boldsymbol{r})$ and integrate over the discontinuity region. Again making use of the orthogonality relations of the vector wave functions and after a long series of algebraic manipulations (see the Appendix), an infinite system of equations is obtained in the form

$$\sum_{i=1}^{2} R_m(k_{n'}, \xi_i, \xi_j) c_{m,n,i} = Q_m(v, k_{n'}, \xi_j) + \sum_{n=-\infty}^{+\infty} \sum_{i=1}^{2} c_{m,n,i} K_m(n, i/n', j) \quad (17)$$

where R_m and Q_m are readily computed and are given in the Appendix and

$$K_m(n, i/n', j) = \int_{-\infty}^{\infty} dk F_m(n, i/n', j/k) \quad (18)$$

where $F_m(n, i/n', j/k)$ is defined in the Appendix.

It is observed that (17) is decoupled with respect to the m integers due to the orthogonality of the $\exp(im\varphi)$ functions on the gyroelectric cross-section area. A prerequisite to solving (17) is to compute the $K_m(n, i/n', j)$ terms with sufficient accuracy. To this end, it is necessary to employ numerical techniques for the computation of the integral in (18).

V. Computation of the $K_m(n, i/n', j)$ Integrals

Before proceeding with the details of the numerical integration of the $K_m(n, i/n', j)$ integrals, it is useful to expose some symmetry relations that the system coupling coefficients possess. It can be verified directly that the $K_m(n, i/n', j)$ term is not symmetric in the strict sense, i.e., $K_m(n, i/n', j) \neq K_m(n', j/n, i)$. This in fact is due to the anisotropy of the discontinuity region. However, it is interesting to notice that interchanging the pairs of parameters (n, n') and (ξ_i, ξ_j) and also replacing the weighting factors $\{B_M(n, \xi_i), B_N(n, \xi_i), B_Q(n, \xi_i)\}$ with $\{-A_M(n', \xi_j), A_N(n', \xi_j), A_Q(n', \xi_j)\}$, the same coupling $K_m(n, i/n', j)$ kernel function is obtained since $\overline{G}(\boldsymbol{r}, \boldsymbol{r}') = \overline{G}(\boldsymbol{r}', \boldsymbol{r})$ (see (7)), i.e., the Green's dyadic is symmetric. This symmetry can be proved easily for the part of the kernels corresponding to the $\overline{G}_1$ part of the Green's function (see (9)). A rather longer algebra is required to prove the symmetry for the part of the matrix elements that originates from the free-space dyadic $\overline{G}_0$.

Furthermore, this relation could be used as an independent check for the numerical algorithms and could also be employed to speed up the numerical computations. To this end, even–odd symmetry relations are also employed for the integrand function, so that the integration range is reduced from $-\infty < k < +\infty$ to $0 < k < +\infty$. Since a truncation is required for the upper bound of the integral, it is necessary to examine the asymptotic behavior of the integrand function as $k \to +\infty$. Introducing the asymptotic expressions for the functions involved, it is shown that the integrand function behaves as k^{-2} as $k \to +\infty$. Therefore, the integral is convergent. The single valuedness of the integrand function is insured by following the branch cuts defined in [5]. The surface-wave pole $k = v$ of the HE_{11} mode is determined by using the successive bisections method up to a six-digit accuracy. The integrand function has a singularity at the $k = v$ point, and an infinitesimal semicircle is used to encircle the surface-wave pole. The final result amounts to the principal value of the integral by excluding the short interval $v - \epsilon < k < v + \epsilon$ $(\epsilon \to 0^+)$ around the pole, plus the half residue contribution from the pole at $k = v$.

A careful examination of the integrand as $k \to k_0$ shows that the integrand function is regular at that point, while as $k \to k_1$ $(\alpha_1 \to 0)$ it behaves as $E_0 + E_1\alpha_1^2 + \cdots$. A Simpson rule numerical integration procedure is adopted for the numerical computation of the integrals. High accuracy is insured by dividing the integration domain into subintervals and performing independent convergence tests for each subinterval.

It is evident from the above considerations that the numerical evaluation of the coupling coefficients is not so easy. Use of the symmetry properties of the matrix elements has been made and effective numerical techniques have been employed to reduce the numerical cost of the computations.

VI. Scattering Coefficients

Assuming that the electric field inside the gyroelectric discontinuity has been evaluated by inverting the linear system (17), it is possible to determine the field anywhere by appropriately applying the fundamental integral (6). The guided-wave complex amplitudes in the forward $(z \to +\infty)$ and backward $(z \to -\infty)$ directions, known as the transmission and reflection coefficients, respectively, are the most interesting quantities for this scattering process. To this end, substitute the expansion of (14) into (6) and assume that the observation point $\boldsymbol{r}$ is inside the dielectric waveguide $(\rho < b)$, but outside the discontinuity region.

Then the following expression is obtained:

$$\boldsymbol{E}(\boldsymbol{r}) = \boldsymbol{E}_0(\boldsymbol{r}) + \iiint_{V_0} d\boldsymbol{r}' \{ \bar{\boldsymbol{G}}_0(\boldsymbol{r}/\boldsymbol{r}') + \bar{\boldsymbol{G}}_1(\boldsymbol{r}/\boldsymbol{r}') \} \cdot \sum_{\iota=1}^{2} \sum_{n=-\infty}^{+\infty} c_{m,n,\iota} \cdot i^m \Big\{ B_M(n,\xi_\iota) \boldsymbol{M}^{(1)}_{m,k_n}(\boldsymbol{r}', K_\iota) + B_N(n,\xi_\iota) \boldsymbol{N}^{(1)}_{m,k_n}(\boldsymbol{r}', K_\iota) + B_Q(n,\xi_\iota) \boldsymbol{Q}^{(1)}_{m,k_n}(\boldsymbol{r}', K_\iota) \Big\}. \quad (19)$$

Consider first the part of the integral that corresponds to the free-space part $\bar{\boldsymbol{G}}_0(r, r')$ of the Green's function. It can easily be shown that, as $|z| \to +\infty$, $\bar{\boldsymbol{G}}_0$ behaves as $\exp(ik_1|\boldsymbol{r}|)/|\boldsymbol{r}|$. Since, in the present work, the interest is focused on guided waves only, the corresponding contribution, diminishing as $1/z$, is neglected. Performing the integration corresponding to the $\bar{\boldsymbol{G}}_1(\boldsymbol{r}/\boldsymbol{r}')$ term, (19) yields

$$\boldsymbol{E}(\boldsymbol{r}) = \boldsymbol{E}_0(\boldsymbol{r}) + \frac{i\alpha}{2} \sum_{n=-\infty}^{+\infty} \sum_{\iota=1}^{2} i^m C_{m,n,\iota} \cdot \int_{-\infty}^{+\infty} dk \frac{1}{\alpha_1^2} \frac{\sin(\alpha k - n\pi)}{\alpha k - n\pi} \cdot \{ [\alpha(m,k) U_m(\alpha_1,\xi_\iota) + b(m,k) V_m(\alpha_1,\xi_\iota)] \cdot \boldsymbol{M}^{(1)}_{m,k}(\boldsymbol{r}, k_1) + [b(m,k) U_m(\alpha_1,\xi_\iota) + c(m,k) V_m(\alpha_1,\xi_\iota)] \boldsymbol{N}^{(1)}_{m,k}(\boldsymbol{r}, k_1) \} \quad (20)$$

where

$$U_m(\alpha_1,\xi_\iota) = B_M(n,\xi_\iota) F_m^{(1)}(\alpha_1,\xi_\iota) + B_N(n,\xi_\iota) \frac{mk_n}{K_\iota} F_m^{(2)}(\alpha_1,\xi_\iota) \quad (21)$$

$$V_m(\alpha_1,\xi_\iota) = B_M(n,\xi_\iota) \frac{mk}{k_1} F_m^{(2)}(\alpha_1,\xi_\iota) + B_N(n,\xi_\iota) \frac{kk_n}{k_1 K_\iota} F_m^{(1)}(\alpha_1,\xi_\iota) + \frac{\alpha_1^2}{k_1} \left[B_N(n,\xi_\iota) \frac{\xi_\iota^2}{K_i} + B_Q(n,\xi_\iota) \right] F_m^{(3)}(\alpha_1,\xi_\iota) \quad (22)$$

where $F_m^{(j)}(x, y)(j = 1,2,3)$ are defined in the Appendix. One can easily observe the existence of a common factor $\exp(ikz)$ in the integrand function of (20). It is because of this rapidly oscillating factor (as $|z| \to +\infty$), that the integral in (20) can be computed asymptotically applying the well-known steepest descent method of integration. After a routine procedure and by neglecting the contributions exhibiting an $\exp(ikz)/z$ behavior, the end result for the guided-wave complex amplitudes originates mainly from the residue contributions of the possible surface-wave poles v. Assuming a single mode ($HE_{\pm 11}$) carrying dielectric waveguide, the final result is written as

$$\underset{z \to +\infty}{\boldsymbol{E}(\boldsymbol{r})} \approx \boldsymbol{E}_0^{\pm 1}(\boldsymbol{r}) \{ 1 + \tau_\pm(v) \} \quad (23)$$

where

$$\tau_\pm(v) = \mp i\pi\alpha \sum_{n=-\infty}^{+\infty} \sum_{\iota=1}^{2} c_{\pm 1,n,\iota} \frac{1}{\sigma^2} \cdot \frac{\sin(\alpha v - n\pi)}{\alpha v - n\pi} \operatorname*{Res}_{k \to v} \{ \alpha(m,k) \} \cdot \Bigg\{ B_M(n,\xi_\iota) F_1^{(1)}(\sigma,\xi_\iota) + \frac{k_n}{K_\iota} B_N(n,\xi_\iota) F_1^{(2)}(\sigma,\xi_\iota) \pm \delta_1(v) \Bigg[B_M(n,\xi_\iota) \frac{v}{k_1} F_1^{(2)}(\sigma,\xi_\iota) + B_N(n,\xi_\iota) \frac{vk_n}{k_1 K_\iota} F_1^{(1)}(\sigma,\xi_\iota) + \frac{\sigma^2}{k_1} \left(B_N(n,\xi_\iota) \frac{\xi_\iota^2}{K_i} + B_Q(n,\xi_\iota) \right) F_1^{(3)}(\sigma,\xi_\iota) \Bigg] \Bigg\}$$

$$\sigma = \left(k_1^2 - v^2 \right)^{1/2} \quad (24)$$

and the (+) or (−) sign corresponds to the HE_{11} ($m = +1$) or $HE_{-11}(m = -1)$ incident wave $\boldsymbol{E}_0^m(\boldsymbol{r})$. The result for the reflected guide wave is obtained in a similar way and is given as

$$\underset{z \to -\infty}{\boldsymbol{E}(\boldsymbol{r})} = \boldsymbol{E}_0^{\pm 1}(\boldsymbol{r}) + \rho_\pm(v) \cdot \left[\boldsymbol{M}^{(1)}_{\pm 1,-v}(\boldsymbol{r}, k_1) \mp \delta_1(v) \boldsymbol{N}^{(1)}_{\pm 1,-v}(\boldsymbol{r}, k_1) \right] \quad (25)$$

where $\rho_\pm(v) = -\tau_\pm(v)$.

VII. Numerical Results

Numerical computations were performed by applying the analytical results of the previous sections. Both isotropic ($\epsilon_1 \to \epsilon_3$ and $\epsilon_2 \to 0$) and gyroelectric discontinuities in single-mode fibers guiding the dominant HE_{11} mode have been considered.

Several checks were performed to insure the correctness of the developed computer program. These were:

a) convergence and numerical stability tests;
b) validity of the energy conservation theorem;
c) comparison with experimental results concerning an air-gap discontinuity.

To check the numerical stability of the results, numerous computations were made by increasing the order of the integer n in the solution of the infinite system (17). In Table I, a sample convergence pattern for the forward scattering coefficient τ is given. The required order of solution to insure good convergence depends upon the electric length $2k_0\alpha$ of the discontinuity. In the resonance region (that is, $2 \leqslant k_0\alpha \leqslant 4$), a fourth-order solution was found sufficient to provide accuracy.

In all the examined cases, the expected nonviolation of the energy conservation theorem was checked. If the power of the incident wave $\boldsymbol{E}_0^{\pm 1}(\boldsymbol{r})$ is denoted by $W_0^\pm$, then the power $W_L^\pm$ consumed for radiation in the single-mode

TABLE I
CONVERGENCE PATTERN FOR THE τ FORWARD SCATTERING COEFFICIENT FOR AN ISOTROPIC SCATTERERS WITH $\epsilon_r = 2.1$, $\epsilon_1 = \epsilon_3 = 3.6$, $\epsilon_2 = 0$, $k_0 b = 2.0$.

$k_0\alpha$ \ N	2	3	4
2.0	−.239 + i.526	−.240+i.527	−.240+i.527
3.0	−.408 − i.141	−.405−i.137	−.406−i.137
5.0	−.854 + i.801	−.118 +i.115	−.118+ i .113

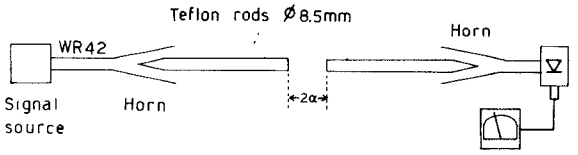

Fig. 2. Experimental setup for the measurement of the insertion loss due to an air-gap discontinuity in a fiber waveguide.

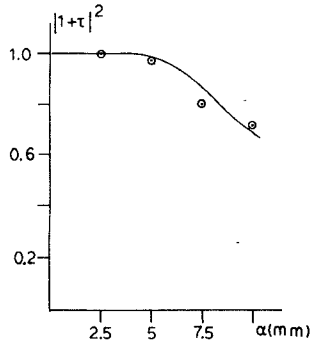

Fig. 3. Comparison between theoretical and experimental results for an air-gap discontinuity in a fiber with $\epsilon_r = 2.1$, $b = 4.25$ mm at $f = 20.5$ GHz.

guide is computed from

$$W_L^{\pm} = W_0^{\pm}\left(1 - |1 + \tau_{\pm}|^2 - |\rho_{\pm}|^2\right).$$

In all the cases examined, the radiation loss $W_L^{\pm}/W_0^{\pm}$ obtained values between 0 and 1, as it is imposed by the energy conservation principle.

In order to have an independent check, results obtained by using the present analysis were compared with measured experimental results for an air-gap discontinuity in a dielectric-rod waveguide. The experimental setup shown in Fig. 2 was used to measure the insertion loss of an air-gap discontinuity in a teflon-rod waveguide at 20.5 GHz. In Fig. 3, a comparison between theoretical and experimental results is presented and a reasonably good agreement is observed.

A. Isotropic Discontinuities

The effect of introducing a longitudinal isotropic ($\epsilon_1 = \epsilon_3 = \epsilon_r'$, $\epsilon_2 = 0$) discontinuity in a single-mode carrying fiber guide was examined. Because of the reciprocal nature of

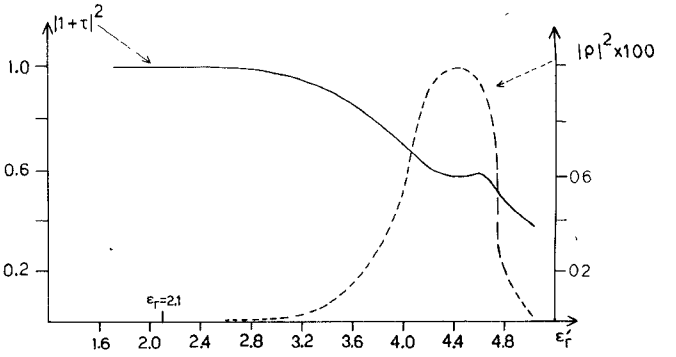

Fig. 4. Variation of the forward $|1+\tau|^2$ and backward $|\rho|^2$ power coefficients with ϵ_r', when $k_0\alpha = k_0 b = 2.0$, $\epsilon_r = 2.1$.

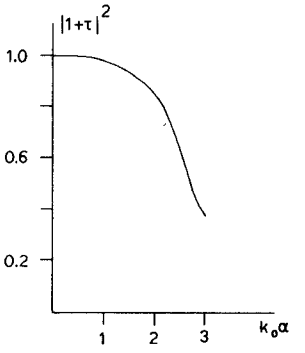

Fig. 5. Variation of the forward $|1+\tau|^2$ power coefficient with $k_0\alpha$, when $k_0 b = 2.0$, $\epsilon_r = 2.1$, and $\epsilon_r' = 3.6$.

the isotropic scatterer, the scattering coefficients $\tau_+(v)$ and $\rho_+(v)$ should be equal to $\tau_-(v)$ and $\rho_-(v)$, respectively (see (24) and (25)). Indeed, this fact was verified by the numerical results. In Fig. 4, the variation of the forward $|1+\tau|^2$ and backward $|\rho|^2$ power coefficients with respect to the relative dielectric constant of the discontinuity region ϵ_r' are shown. In this case, the fiber waveguide characteristics were $\epsilon_r = 2.1$ and $k_0\alpha = k_0 b = 2.0$ and, as it can be observed from the figure, in case $\epsilon_r' \approx \epsilon_r$, the effect of the discontinuity is negligible and only when $\epsilon_r'/\epsilon_r > 1.6$ does the scattering become significant.

A similar picture is observed in Fig. 5, when the discontinuity electric length $k_0\alpha$ is varied for constant $\epsilon_r' = 3.6$, $\epsilon_r = 2.1$, and $k_0 b = 2.0$ values.

B. Gyroelectric Discontinuities

In treating the scattering of a propagating HE_{11} wave from a gyroelectric discontinuity, the z-component (E_z) of the incident wave is assumed to have a $\cos\varphi$ azimuthal dependence. Then, according to the superposition principle, the scattered E_z component in the forward direction will have a φ-dependence of the form

$$\frac{1+\tau_+}{2}e^{i\varphi} + \frac{1+\tau_-}{2}e^{-i\varphi} = \left(1 + \frac{\tau_+ + \tau_-}{2}\right)\cos\varphi + i\frac{\tau_+ - \tau_-}{2}\sin\varphi. \quad (26)$$

Therefore, gyroelectric discontinuities modify the polariza-

tion of the incident wave, and, in general, elliptically polarized waves are obtained. In order to characterize the polarization of the forward scattered waves, a complex ellipticity ratio is defined as

$$g = \frac{\tau_+ - \tau_-}{2 + \tau_+ + \tau_-}. \tag{27}$$

In addition, the forward scattered wave power coefficient is determined as

$$T = \frac{|1+\tau_+|^2}{2} + \frac{|1+\tau_-|^2}{2}. \tag{28}$$

TABLE II
POLARIZATION ELLIPTICITY RATIO (g) AND FORWARD SCATTERED WAVE POWER COEFFICIENT (T) VALUES FOR $\epsilon_r = 2.1$, $k_0\alpha = 4.0$, $k_0 b = 2.0$, $\epsilon_3 = 2.1$, $\epsilon_1 = 0.675$, AND VARIOUS ϵ_2 OFF-DIAGONAL TENSOR ELEMENTS

ε_2	g	T
0.123	34.7|33.9°	0.170
0.245	1.10|-70.5°	0.245
0.369	0.79|-74.9°	0.413
0.492	0.61|-74°	0.558
0.615	0.49|-71.7°	0.663

TABLE III
VARIATION OF $\tau_\pm, g, T$, WITH k_0 FOR TWO ANISOTROPIC SCATTERERS WITH $\epsilon_r = 2.1$, $\epsilon_1 = 0.675$, $\epsilon_2 = 0.247$, $k_0 b = 2.0$

$\varepsilon_3 = 2.1$

$k_0\alpha$	τ_+ τ_-	g		T
1.0	(-.723-i81.58)10^{-4} (.313+i34.29)10^{-4}	5.8 X 10^{-3}	89.6°	.999
2.0	-128-i.133 (-140+i.109) 10^{-3}	6.7 X 10^{-2}	88.4°	.996
3.0	-.191-i.442 -.185-i.171	.156 -	70.6°	.772

$\varepsilon_3 = 1.0$

$k_0\alpha$	τ_+ τ_-	g		T
2.0	-.145-i.138 (-.571-i.380)10^{-2}	6.72 X 10^{-3}	49.2°	.98
3.0	-.201-i.445 -.206-i.191	.148	-67.1°	.75
4.0	-.594-i.335 -.528+i.116	.504	-84°	.25

Several types of dielectric constant tensors have been considered. In Table II, results are given for a gyroelectric discontinuity with $\epsilon_1 = 0.675$, $\epsilon_3 = 2.1$, $k_0\alpha = 4.0$, $k_0 b = 2.0$, $\epsilon_r = 2.1$, and for various ϵ_2 values. The variation of the g ratio is interesting, especially when $\epsilon_2 = 0.123$. In this case, the scattered wave is almost orthogonally polarized to the incident wave. However, the forward scattered wave power is quite small.

The variation of g and T with respect to the gyroelectric discontinuity length has also been examined. In Table III, results are given for two types of $\bar{\epsilon}$-tensor permittivity values, where in the resonance region (i.e., $k_0\alpha \geq 3$), strong depolarization can be observed. Although only ideal gyroelectric media are considered here, the present analysis can be applied to study millimeter-wave structures with solid-state plasmas in semiconductor crystals under an axial magnetic field of the type described in [7].

VIII. CONCLUSIONS

The diffraction of guided waves from a finite-length discontinuity inside a fiber waveguide has been analyzed using an integral equation method. A gyrotropic tensor dielectric permittivity is considered. Therefore, the analysis also covers the case of isotropic discontinuities in fiber waveguides. The theory has been compared with experimental results concerning an air-gap discontinuity and a good agreement has been verified and several interesting phenomena have been observed.

APPENDIX

Making use of the orthogonality relations of the $\boldsymbol{M}$, $\boldsymbol{N}$, and $\boldsymbol{Q}$ cylindrical wave functions when performing the integration over the discontinuity region, the end result for the $\boldsymbol{I}_{pi}^{(X)}(\boldsymbol{r})$ $(X = M, N, Q)$ integrals after a proper rearrangement can be set in the form

$$\boldsymbol{I}_{pi}^{(M)}(\boldsymbol{r}) = \int_{-\infty}^{+\infty} dk \frac{i}{2\alpha_1^2} \frac{\sin(\alpha(k-k_n))}{k-k_n} \boldsymbol{R}_p^{(M)}(k, \xi_i) + \hat{\rho} \frac{p}{k_1^2} \frac{im}{\rho} J_m(\xi_i \rho) e^{im\varphi} \varphi_n(z)$$

$$\boldsymbol{I}_{pi}^{(N)}(\boldsymbol{r}) = \int_{-\infty}^{+\infty} dk \frac{i}{2\alpha_1^2} \frac{\sin(\alpha(k-k_n))}{k-k_n} \boldsymbol{R}_p^{(N)}(k, \xi_i) + \hat{\rho} \frac{p}{k_1^2} \frac{ik}{K_i} \frac{\partial Jm(\xi_i \rho)}{\partial \rho} e^{im\varphi} \varphi_n(z)$$

$$\boldsymbol{I}_{pi}^{(Q)}(\boldsymbol{r}) = \int_{-\infty}^{+\infty} dk \frac{i}{2\alpha_1^2} \frac{\sin(\alpha(k-k_n))}{k-k_n} \boldsymbol{R}_p^{(Q)}(k, \xi_i), \qquad p = 0, 1, \quad i = 1, 2$$

where $\boldsymbol{R}_p^{(X)}(k, \xi_i)$ $(X = M, N, Q)$ can be arranged as a combination of the cylindrical wave functions $\boldsymbol{M}$, $\boldsymbol{N}$, and $\boldsymbol{Q}$, and $\varphi_n(z)$ is given by

$$\varphi_n(z) = \pi e^{ik_n z} - \int_{-\infty}^{+\infty} dk \frac{\sin(\alpha(k-k_n))}{k-k_n} e^{ikz}.$$

One can observe that, for $-\alpha \leq z \leq \alpha$, $\varphi_n(z) = 0$. This

observation is critical, since the method of moments can be straightforward applied to the remaining part of $\boldsymbol{I}_{pl}^{(X)}(\boldsymbol{r})$ to obtain the infinite system (17).

The R_m and Q_m are given from

$$R_m(k_{n'},\xi_l,\xi_j)=\Bigg\{-A_M(n',\xi_l)A_M(n',\xi_j)+A_N(n',\xi_l)A_N(n',\xi_j)\frac{k_{n'}^2}{K_lK_j}\Bigg\}F_m^{(1)}(\xi_l,\xi_j)+mk_{n'}\Bigg\{A_M(n',\xi_l)A_N(n',\xi_j)\frac{1}{K_j}-A_M(n',\xi_j)A_N(n,\xi_l)\frac{1}{K_l}\Bigg\}F_m^{(2)}(\xi_l,\xi_j)+\Bigg\{A_N(n',\xi_l)\frac{\xi_l^2}{K_l}+A_Q(n',\xi_l)\Bigg\}\cdot\Bigg\{A_N(n',\xi_j)\frac{\xi_j}{K}+A_Q(n',\xi_j)\Bigg\}F_m^{(3)}(\xi_l,\xi_j)$$

$$Q_m(v,k_{n'},\xi_j)=i^m\frac{\sin(\alpha v-n'\pi)}{\alpha v-n'\pi}\Bigg[\Bigg\{-A_M(n',\xi_j)+\delta_m(v)\frac{k_{n'}v}{K_jk_1}A_N(n',\xi_j)\Bigg\}F_m^{(1)}(\delta,\xi_j)+m\Bigg\{-\delta_m(v)\frac{v}{k_1}A_M(n',\xi_j)+\frac{k_{n'}}{K_j}A_N(n',\xi_j)\Bigg\}F_m^{(2)}(\sigma,\xi_j)+\delta_m(v)\frac{v^2}{k_1}\Bigg\{\frac{\xi_j^2}{K_j}A_N(n',\xi_j)+A_Q(n',\xi_j)\Bigg\}F_m^{(3)}(\sigma,\xi_j)\Bigg]$$

where $\sigma=(k_1^2-v^2)^{1/2}$ and $F_m^{(p)}(x,y)$ $(p=1,2,3)$ are

The integral in (18) is given as

$$\begin{aligned}K_m(n,i/n',j)&=\int_{-\infty}^{+\infty}dk\,\frac{i\alpha}{2\alpha_1^2}\frac{\sin(\alpha k-n\pi)}{\alpha k-n\pi}\frac{\sin(\alpha k-n'\pi)}{\alpha k-n'\pi}\\&\cdot\Big[B_m(n,\xi_l)\{-A_M(n',\xi_j)\phi_{MM}(k)+A_N(n',\xi_j)\phi_{MN}(k)+A_Q(n',\xi_j)\phi_{MQ}(k)\}\\&\cdot B_N(n,\xi_i)\{-A_M(n',\xi_j)\phi_{NM}(k)+A_N(n',\xi_j)\phi_{NN}(k)+A_Q(n',\xi_j)\phi_{NQ}(k)\}\\&\cdot B_Q(n,\xi_l)\{-A_M(n',\xi_j)\phi_{QM}(k)+A_N(n',\xi_j)\phi_{QN}(k)+A_Q(n',\xi_j)\phi_{QQ}(k)\}\\&+\alpha(m,k)\{B_M(n,\xi_l)F_m^{(1)}(\alpha_1,\xi_l)+mk_nB_N(n,\xi_l)F_m^{(2)}(\alpha_1,\xi_l)\}\\&\cdot\{-A_M(n',\xi_j)F_m^{(1)}(\alpha_1,\xi_j)+mk_nA_N(n',\xi_j)F_m^{(2)}(\alpha_1,\xi_j)\}\\&+\frac{1}{k_1}b(m,k)\Big\{B_M(n,\xi_l)mkF_m^{(2)}(\alpha_1,\xi_l)\\&+kk_nB_N(n,\xi_i)F_m^{(1)}(\alpha_1,\xi_i)+\alpha_1^2\big[\xi_i^2B_N(n,\xi_i)\\&+B_Q(n,\xi_i)\big]F_m^{(3)}(\alpha_1,\xi_i)\Big\}\\&\cdot\{-A_M(n',\xi_j)F_m^{(1)}(\alpha_1,\xi_j)+mk_{n'}A_N(n',\xi_j)F_m^{(2)}(\alpha_1,\xi_j)\}\\&+\frac{1}{k_1}b(m,k)\{B_M(n,\xi_l)F_m^{(1)}(\alpha_1,\xi_l)+mk_nB_N(n,\xi_l)F_m^{(2)}(\alpha_1,\xi_l)\}\\&\{-A_M(n',\xi_j)mkF_m^{(2)}(\alpha_1,\xi_j)\end{aligned}$$

$$\begin{pmatrix}G_m^{(1)}(x,y)\\F_m^{(1)}(x,y)\end{pmatrix}=\frac{xyb}{x^2-y^2}\begin{Bmatrix}xJ_m'(yb) & H_m(xb) & -yJ_m(yb) & H_m'(xb)\\ & J_m(xb) & & J_m'(xb)\end{Bmatrix}$$

$$\begin{pmatrix}G_m^{(2)}(x,y)\\F_m^{(2)}(x,y)\end{pmatrix}=J_m(yb)\begin{matrix}H_m(xb)\\J_m(xb)\end{matrix}$$

$$\begin{pmatrix}G_m^{(3)}(x,y)\\F_m^{(3)}(x,y)\end{pmatrix}=\frac{b}{x^2-y^2}\begin{Bmatrix}yJ_m'(yb) & H_m(xb) & -xJ_m(yb) & H_m'(xb)\\ & J_m(xb) & & J_m'(xb)\end{Bmatrix}.$$

$$+ kk_{n'}A_N(n',\xi_j)F_m^{(1)}(\alpha_1,\xi_j)$$
$$+ \alpha_1^2\left[\xi_j^2 A_N(n',\xi_j)+A_Q(n',\xi_j)\right]F_m^{(3)}(\alpha_1,\xi_j)\Big\}$$
$$+\frac{1}{k_1^2}c(m,k)\Big\{B_M(n,\xi_i)mkF_m^{(2)}(\alpha_1,\xi_i)$$
$$+ kk_nB_N(n,\xi_i)F_m^{(1)}(\alpha_1,\xi_i)+\alpha_1^2\left[\xi_i^2B_N(n,\xi_i)\right.$$
$$\left.+B_Q(n,\xi_i)\right]F_m^{(3)}(\alpha_1,\xi_i)\Big\}$$
$$\cdot\Big\{-A_M(n',\xi_j)mkF_m^{(2)}(\alpha_1,\xi_j)$$
$$+ kk_{n'}A_N(n',\xi_i)F_m^{(1)}(\alpha_1,\xi_j)$$
$$+\alpha_1^2\left[\xi_j^2A_N(n',\xi_j)+A_Q(n',\xi_j)\right]F_m^{(3)}(\alpha_1,\xi_j)\Big\}\Big]$$

$$B_M(n,\xi_i)=k_0^2(\epsilon_1-\epsilon_r)A_M(n,\xi_i)$$
$$+k_0^2\epsilon_2A_N(n,\xi_i)/K_i$$
$$B_N(n,\xi_i)=k_0^2(\epsilon_1-\epsilon_r)A_N(n,\xi_i)$$
$$+k_0^2\epsilon_2A_M(n,\xi_i)K_i/k_n$$
$$B_0(n,\xi_i)=k_0^2(\epsilon_1-\epsilon_r)A_Q(n,\xi_i)+k_0^2(\epsilon_3-\epsilon_1)$$
$$\cdot\left\{A_Q(n,\xi_i)+\frac{\xi_i^2}{K_i}A_N(n,\xi_i)\right\}$$
$$-k_0^2\epsilon_2\xi_i^2A_M(n,\xi_i)/k_n$$

$$\phi_{MM}(k)=G_m^{(1)}(\alpha_1,\xi_i)F_m^{(1)}(\alpha_1,\xi_j)$$
$$+\frac{m^2k^2}{k_1^2}G_m^{(2)}(\alpha_1,\xi_i)F_m^{(2)}(\alpha_1,\xi_i)$$
$$+\frac{2i}{\pi}\frac{\alpha_1^2}{\alpha_1^2-\xi_i^2}F_m^{(1)}(\xi_i,\xi_j)$$

$$\phi_{MN}(k)=\phi_{MN}(k,k_n,k_{n'},\xi_i,\xi_j)$$
$$=mk_{n'}G_m^{(1)}(\alpha_1,\xi_i)F_m^{(2)}(\alpha_1,\xi_j)$$
$$+mk_{n'}\frac{k^2}{k_r^2}G_m^{(2)}(\alpha_1,\xi_i)F_m^{(1)}(\alpha_1,\xi_j)$$
$$+mk\alpha_1^2\frac{\xi_j^2}{k_1^2}G_m^{(2)}(\alpha_1,\xi_i)F_m^{(3)}(\alpha_1,\xi_j)$$
$$+\frac{2i}{\pi}\frac{\alpha_1^2}{\alpha_1^2-\xi_i^2}mk_{n'}F_m^{(2)}(\alpha_1,\xi_j)$$

$$\phi_{MQ}(k)=\phi_{MQ}(k,k_n,k_{n'},\xi_i,\xi_j)$$
$$=mk\frac{\alpha_1^2}{k_1^2}G_m^{(2)}(\alpha_1,\xi_i)F_m^{(3)}(\alpha_1,\xi_j)$$

$$\phi_{NN}(k)=m^2k_nk_{n'}G_m^{(2)}(\alpha_1,\xi_i)F_m^{(2)}(\alpha_1,\xi_j)$$
$$+\frac{k^2}{k_1^2}k_nk_{n'}G_m^{(1)}(\alpha_1,\xi_i)F_m^{(1)}(\alpha_1,\xi_j)$$
$$+kk_{n'}\frac{\xi_i^2\alpha_1^2}{k_1^2}G_m^{(3)}(\alpha_1,\xi_i)F_m^{(1)}(\alpha_1,\xi_j)$$
$$+kk_n\frac{\xi_j^2\alpha_1^2}{k_1^2}G_m^{(2)}(\alpha_1,\xi_i)F_m^{(3)}(\alpha_1,\xi_j)$$
$$+\frac{\xi_1^2\xi_j^2\alpha_1^2}{k_1^2}G_m^{(3)}(\alpha_1,\xi_i)F_m^{(3)}(\alpha_1,\xi_j)$$
$$+\frac{2i}{\pi}\frac{1}{k_1^2}\frac{\alpha_1^2}{\alpha_1^2-\xi_i^2}\Big\{k_{n'}\left[k_n\left(k_1^2-\xi_i^2\right)+k\xi_i^2\right]$$
$$\cdot F_m^{(1)}(\xi_i,\xi_j)+\xi_i^2\xi_j^2\left(kk_n+\alpha_1^2\right)F_m^{(3)}(\xi_i,\xi_j)\Big\}$$

$$\phi_{MN}(k)=\phi_{NM}(k,k_{n'},k_n,\xi_j,\xi_i)$$

$$\phi_{NQ}(k)=\phi_{NO}(k,k_n,k_{n'},\xi_i,\xi_j)$$
$$=kk_n\frac{\alpha_1^2}{k_1^2}G_m^{(1)}(\alpha_1,\xi_i)F_m^{(3)}(\alpha_1,\xi_j)$$
$$+\frac{\xi_i^2\alpha_1^4}{k_1^2}G_m^{(3)}(\alpha_1,\xi_i)F_m^{(3)}(\alpha_1,\xi_j)$$
$$+\frac{2i}{\pi}\frac{1}{k_1^2}\frac{\alpha_1^2}{\alpha_1^2-\xi_i^2}\xi_i^2\left(kk_n+\alpha_1^2\right)F_m^{(3)}(\xi_i,\xi_j)$$

$$\phi_{QM}(k)=\phi_{MQ}(k,k_{n'},k_n,\xi_j,\xi_i)$$

$$\phi_{QN}(k)=\phi_{NQ}(k,k_{n'},k_n,\xi_j,\xi_i)$$

$$\phi_{QQ}(k)=\frac{\alpha_1^4}{k_1^2}G_m^{(3)}(\alpha_1,\xi_i)F_m^{(3)}(\alpha_1,\xi_j)$$
$$+\frac{2i}{\pi}\frac{1}{k_1^2}\frac{\alpha_1^2}{\alpha_1^2-\xi^2}F_m^{(3)}(\xi_i,\xi_j).$$

References

[1] S. Wang, J. D. Crow, and M. Shah, "Thin-film optical-waveguide mode converters using gyrotropic and anisotropic substrates," *Appl. Phys. Lett.*, vol. 19, pp. 187–189, 1971.

[2] J. M. Hammer, "Modulation and switching of light in dielectric waveguides," in *Integrated Optics*, T. Tamir Ed. New York: Springer-Verlag, 1979, pp. 139–200.

[3] R. C. Alferness, "Waveguide electrooptic modulators," *IEEE Trans. Microwave Theory Tech.*, vol. MTT-30, pp. 1121–1137, 1982.

[4] A Shibukawa, A. Katsui, H. Iwamura, and S. Hayashi, "Compact optical isolator for near-infrared radiation," *Electron. Lett.*, vol. 13, pp. 721–722, 1977.

[5] N. K Uzunoglu, "Scattering from inhomogeneities inside a fiber waveguide," *J. Op. Soc. Amer.*, vol. 71, pp. 259–273, 1981.

[6] P. H. Pathak, "On the eigenfunction expansion of electromagnetic dyadic Green's function," *IEEE Trans. Antennas Propagat.*, vol. 31, June 1983.

[7] H. J. Kung, "Solid-state microwave and millimeter-wave sources development—A personal account," *IEEE Trans. Microwave Theory Tech.*, vol. MTT-32, pp. 1083–1087, 1984.

✠

P. G. Cottis was born in Salonica, Greece, in 1956. He received the Diploma degree in electrical engineering from the National Technical University of Athens (NTUA) in 1979, the M.Sc.

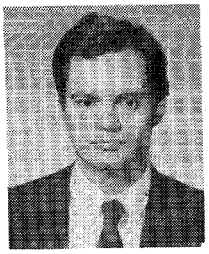

degree in communication engineering from the University of Manchester (UMIST) in 1980, and the Doctor's degree in electrical engineering from NTUA in 1984.

Since 1981, he has been working as a Research Associate in the Department of Electrical Engineering at NTUA. His main research interest is in the electromagnetic fields area with emphasis on scattering and propagation at millimeter and optical wavelengths.

Nikolaos K. Uzunoglu (M'82) was born on June 19, 1951. He received the B.Sc. in electrical engineering in 1973. He obtained the M.Sc. and Ph.D. degrees from the University of Essex, England, in 1974 and 1976, respectively. He also obtained the D.Sc. degree in 1982 from the National Technical University of Athens, Greece.

From 1977 to 1984, he worked as a Research Scientist with the Hellenic Navy Technology Development Office. In May 1984, he was elected Associate Professor of Microwaves and Fiber Optics at the National Technical University of Athens, where he is presently serving. His main fields of interest include scattering of electromagnetic waves, antenna design, millimeter waves, and fiber optics.

Dr. Uzunoglu is a member of the Optical Society of America.